ACS APPLIED MATERIALS & INTERFACES

Research Article

Cite This: ACS Appl. Mater. Interfaces 2017, 9, 42482−42491

www.acsami.org

Nitrogen-Doped Porous Carbon-ZnO Nanopolyhedra Derived from ZIF-8: New Materials for Photoelectrochemical Biosensors

Ruiying Yang, Xiaoxia Yan, Yanmei Li, Xiaohua Zhang, and Jinhua Chen*

State Key Laboratory of Chemo/Biosensing and Chemometrics, College of Chemistry and Chemical Engineering, Hunan University, Changsha 410082, P. R. China

Supporting Information

ABSTRACT: Herein, novel photoactive materials, nitrogen-doped porous carbon-ZnO (NPC-ZnO) nanopolyhedra, were prepared by direct carbonization of zeolitic imidazolate framework (ZIF)-8 nanopolyhedra in a nitrogen atmosphere. The morphology, structure, and photoelectrochemical (PEC) properties were characterized by scanning electron microscopy, transmission electron microscopy, X-ray photoelectron spectroscopy, Raman spectroscopy, nitrogen adsorption−desorption method, and PEC methods. The results showed that the obtained NPC-ZnO nanopolyhedra had a rhombic dodecahedron morphology with uniform particle size of about 100 nm and a high surface area of 609.2 m^2 g^{-1}. Under visible-light irradiation, the NPC-ZnO nanopolyhedra showed better PEC performance than ZnO nanorod and the ZIF-8 nanopolyhedra in aqueous media with dissolved oxygen and ascorbic acid. Taking alkaline phosphatase (ALP) as a model, a NPC-ZnO nanopolyhedra-based PEC sensor was developed and showed good performance for ALP assay with a wide linear response range from 2 to 1500 U L^{-1} and a low detection limit of 1.7 U L^{-1}. Moreover, the PEC sensor possessed acceptable selectivity, reproducibility, and stability. The prepared NPC-ZnO nanopolyhedra provide a new photoactive material for the construction of PEC sensors and may have promising applications in PEC assay of heavy metal ions, organic pollutants, and biomolecules.

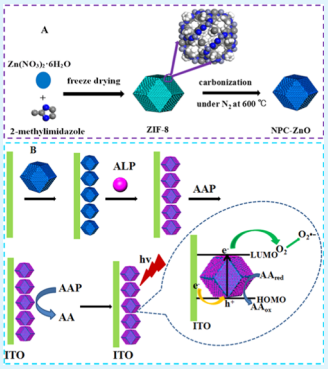

KEYWORDS: *ZIF-8, nitrogen-doped porous carbon-ZnO nanopolyhedra, photoactive material, photoelectrochemical biosensor, alkaline phosphatase*

1. INTRODUCTION

Photoelectrochemical (PEC) analysis is a new analytical method based on photoinduced electron-transfer processes at electrode/solution interfaces.[1−8] Because of the separation of the excitation source and the detection signal,[9,10] the PEC detection possesses potentially high sensitivity and reduced background signals compared with conventional electrochemical and optical methods.[11,12] Meanwhile, on the basis of the utilization of electronic readout, the technique has additional advantages of low cost, simplicity, and easy miniaturization.[13,14] Therefore, the PEC analysis has been widely applied to detect various biomolecules and has attracted considerable research interest.[6,15] However, for the PEC analysis, photoactive material plays a very important role in improving the photoelectric conversion efficiency and obtaining desirable analytical performance. Up to now, varieties of functional materials, such as CdTe,[16,17] CdS,[18,19] ZnO,[20−22] TiO_2,[23,24] C_3N_4,[25,26] BiOI,[27] and Bi_2S_3,[28] have been developed and used to construct PEC sensors. Among them, ZnO nanomaterials have received much attention owing to their high electron mobility and facile synthesis. However, the direct band gap (3.37 eV) of ZnO has limited its light absorption to ultraviolet range, which belongs to less than 5% solar spectrum energy and may inevitably cause the damage of biomolecules.[29,30] To overcome these shortcomings and broaden to visible-light range, semiconductors with narrow band gap or organic photosensitizers were usually employed to modify ZnO nanomaterials.[31] However, for these methods, it is difficult to obtain a uniform sensitization of ZnO nanomaterials and the modification process is complex. On the other hand, it is well known that enhancing the electronic conductivity of ZnO nanomaterials will be beneficial to inhibiting the recombination of photogenerated electron−hole pairs.[32,33] Thus, it is important and necessary to seek new ways to obtain the new sensitization structure of ZnO nanomaterials.

Recently, metal−organic frameworks (MOFs) have received more and more attention and been applied in many areas, such as gas storage, supercapacitors, catalysis, and sensors,[34,35] due to high specific surface area (SSA), high porosity, open cavities, and high degree of synthetic tenability of different metal ions and organic bridging ligands.[36] It was also reported that MOFs could be considered as photoactive materials for the construction of PEC sensors.[37,38] For example, Zhan et al. developed a PEC sensor for the detection of H_2O_2 based on ZnO@zeolitic imidazolate framework (ZIF)-8 nanorod arrays.[37] Zhang et al. reported a PEC sensor based on zirconium-based porphyrinic metal−organic framework for a label-free phosphoprotein detection.[38] However, due to the low

Received: July 24, 2017
Accepted: November 22, 2017
Published: November 22, 2017

DOI: 10.1021/acsami.7b10856
ACS Appl. Mater. Interfaces 2017, 9, 42482−42491

electrical conductivity of MOFs, the photoelectron transfer between photoelectrode and MOFs is difficult, which reduces the response signal of the PEC sensors. Therefore, it is a challenge to find a way to improve the electrical conductivity of MOFs and to make better for their applications in PEC sensor.

In our previous works, it was noted that nitrogen-doped porous carbons (NPCs) derived from ZIF-8 showed excellent electrochemical properties toward ascorbic acid (AA) oxidation and oxygen reduction reaction due to their high specific surface area, porous structure, and high electronic conductance.[39,40] This inspires us to prepare NPC-ZnO nanopolyhedra by the direct carbonization of ZIF-8 (Scheme 1A). The obtained

Scheme 1. (A) Schematic Diagram for the Preparation of NPC-ZnO Nanopolyhedra and (B) Mechanism of NPC-ZnO Nanopolyhedra-Based Photoelectrochemical Biosensor for Alkaline Phosphatase (ALP) Assay

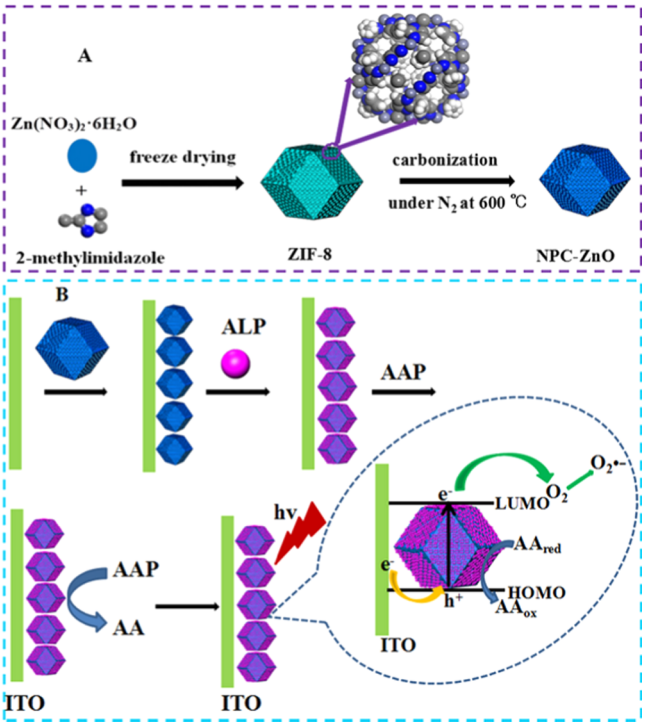

NPC-ZnO nanopolyhedra should enhance the photogenerated electron transfer between the electrode and NPC-ZnO nanopolyhedra because of the excellent electrochemical performance of NPC and uniform distribution of ZnO in the nanopolyhedra. On the other hand, the interaction between NPC and ZnO may change the band gap of ZnO and broaden the light absorption range from ultraviolet to visible light.[41]

On the other hand, alkaline phosphatase (ALP) is extensively studied in clinical practice and commonly used as a significant biochemical label for diagnostics due to its high catalytic activity and low cost.[42,43] The abnormal expression of ALP in the serum is closely correlated with various diseases including liver dysfunction, diabetes, prostatic cancer, bone diseases, and so on.[44,45] Therefore, simple and sensitive assay of ALP is of great significance to a wide range of analytical applications. Although a variety of methods, such as fluorescence,[46,47] chemiluminescence,[48] electrochemiluminescence,[49,50] colorimetry,[51,52] and electrochemistry,[45] have been used for the ALP assay, these approaches usually have some disadvantages including high cost, complex synthesis, or surface modification processes, which greatly limits their practical applications. So, rapid, simple, and sensitive methods for ALP assay are still desired.

Here, taking ALP as a model due to its special importance in clinical diagnostics and biomedical applications, a PEC biosensor was constructed simply by modifying the NPC-ZnO nanopolyhedra onto the indium tin oxide (ITO) electrode surface (Scheme 1B). Compared with the ZnO nanorod and ZIF-8 nanopolyhedra, the ZIF-8-derived NPC-ZnO nanopolyhedra demonstrated super PEC activity, low charge transfer resistance, excellent adsorption capacity, and high visible photocatalytic activity. The developed NPC-ZnO nanopolyhedra-based PEC biosensor showed excellent performance for the ALP assay with wide linear response range and low detection limit.

2. EXPERIMENTAL SECTION

2.1. Materials and Reagents. The indium tin oxide (ITO) slices were obtained from Zhuhai Kaivo Electronic Components Co., Ltd., China (ITO-B001-1), with sheet resistance <10 Ω sq^{-1} and coating thickness of 180 ± 25 nm. ALP was purchased from New England Biolabs, Ltd. (China). Ascorbic acid 2-phosphate sesquimagnesium salt (AAP) was obtained from Sigma-Aldrich. Tris(hydroxymethyl)-aminomethane (Tris) was supplied by Solarbio Science & Technology Co., Ltd. (China). Zinc nitrate hexahydrate, 2-methylimidazole, and ascorbic acid (AA) were purchased from Sinopharm Chemical Reagent Co., Ltd. (China). The normal human serum was bought from Anyan Inc. (China). All of the chemicals were of analytical grade and used without further purification. All of the aqueous solutions were prepared by ultrapure water obtained from a Milli-Q water purification system (18.2 MΩ cm, Millipore Corp., Bedford, MA).

2.2. Apparatus. The morphology and structure of the prepared samples were investigated by scanning electron microscopy (SEM, JSM-6700F, Japan) equipped with an energy-dispersive spectrometer (EDS), transmission electron microscopy (TEM, JEM-2100F, Japan), powder X-ray diffraction (PXRD, D/MAX-RA, Japan), and Raman spectroscopy (Labram-010, JY, France). The types of C, N, O, and Zn were analyzed by X-ray photoelectron spectroscopy (XPS, ESCA-LAB250Xi). The UV−vis absorption spectra were recorded by a UV-2500 UV−vis spectrophotometer (LabTech). Adsorption isotherms of nitrogen and pore structure of the sample were measured using a Micrometrics ASAP 2020 system. A PLS-SXE300 Xe lamp equipped with an optical filter (λ > 420 nm) was used as the light source. Photoelectrochemical and electrochemical measurements were carried out on a CHI 660D electrochemical workstation (China) at room temperature. A typical three-electrode cell was used with a modified ITO electrode (2.8 mm in radius) as the working electrode, a platinum wire as the auxiliary electrode, and a saturated calomel electrode (SCE) as the reference electrode. All of the potentials were referred to SCE. Tris−HCl (0.1 M, pH 8.0) buffer solution was utilized as the supporting electrolyte.

2.3. Preparation of NPC-ZnO Nanopolyhedra. ZIF-8 nanopolyhedra were synthesized according to the previous paper, with slight modification.[40,53] Typically, zinc nitrate hexahydrate (1.485 g) and 2-methylimidazole (3.28 g) were separately dissolved in absolute methanol (50 mL). Then, 2-methylimidazole solution was quickly poured into the zinc nitrate hexahydrate solution under agitation. After that, the resultant mixed solution was stirred for 2 h at room temperature to complete the crystallization process. Finally, the precipitate (ZIF-8 nanopolyhedra) was obtained by centrifugation, washed several times with absolute methanol, and freeze-dried overnight. NPC-ZnO nanopolyhedra were prepared by the direct carbonization of ZIF-8 nanopolyhedra in a tube furnace at 600 °C under N_2 for 3 h with a heating rate of 5 °C min^{-1}. The black powders (NPC-ZnO nanopolyhedra) were obtained and used without any further treatment.

2.4. Preparation of the ITO/NPC-ZnO Electrode. Prior to modification, ITO electrodes were cleaned by ultrasonic treatment for

DOI: 10.1021/acsami.7b10856
ACS Appl. Mater. Interfaces 2017, 9, 42482−42491

15 min in acetone, 1 M NaOH in ethanol/water mixture (v/v, 1:1) and water, respectively, and then dried at 60 °C for 2 h. NPC-ZnO nanopolyhedra (8 mg) were ultrasonically dispersed in water (8 mL), and then 25 μL of NPC-ZnO nanopolyhedra suspension (1 mg mL^{-1}) was dropped onto the cleaned ITO electrode surface. After drying in air, the ITO/NPC-ZnO electrode was obtained. Furthermore, for comparison, the ITO/ZnO and ITO/ZIF-8 electrodes were fabricated with the same process.

2.5. Photoelectrochemical Assay of ALP. CutSmart buffer (20 μL, 1×) containing different concentrations of ALP was dropped onto the ITO/NPC-ZnO electrodes, and then the electrodes were incubated at 4 °C in a moisture atmosphere to avoid evaporation of the solvent. Subsequently, the ITO/NPC-ZnO/ALP electrodes were immersed into the 0.1 M Tris−HCl buffer (pH 8.0) containing a definite concentration of AAP at 37 °C for the PEC analysis.

3. RESULTS AND DISCUSSION

3.1. Characterization of NPC-ZnO Nanopolyhedra. The SEM and TEM images of ZnO nanorods, ZIF-8 nanopolyhedra, and NPC-ZnO nanopolyhedra are shown in Figure 1. From Figure 1A, it is noted that the ZnO nanorods

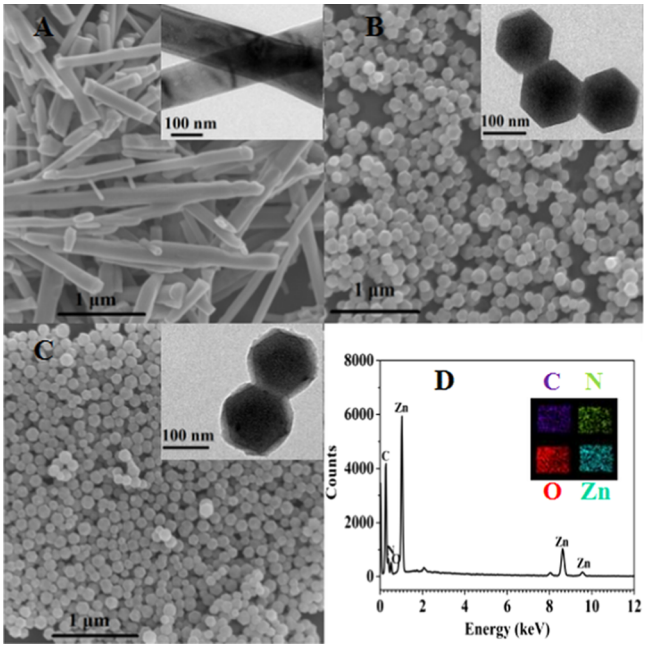

Figure 1. SEM images of (A) ZnO nanorods, (B) ZIF-8 nanopolyhedra, and (C) NPC-ZnO nanopolyhedra. (D) EDS spectrum of NPC-ZnO nanopolyhedra. Insets of (A)−(C) are the corresponding TEM images and the inset of (D) is the corresponding EDS mapping of the NPC-ZnO nanopolyhedra.

have a diameter of about 150 nm. The ZIF-8 nanopolyhedra have the typical rhombic dodecahedron morphology with a uniform particle size of ca. 150 nm (Figure 1B), which is in accordance with that obtained from the reported literatures.[40,53] The NPC-ZnO nanopolyhedra keep the similar morphology of ZIF-8 nanopolyhedra, although the particle size of the NPC-ZnO nanopolyhedra (ca. 100 nm, Figure 1C) is smaller than that of the ZIF-8 nanopolyhedra. On the other hand, the elemental compositions of the NPC-ZnO nanopolyhedra have been investigated by EDS, and the results are shown in Figure 1D. It can be observed that the NPC-ZnO nanopolyhedra have four elements (C, N, O, and Zn) that are distributed uniformly in the sample.

The ZnO nanorods, ZIF-8 nanopolyhedra, and NPC-ZnO nanopolyhedra are further characterized by PXRD (Figure 2A).

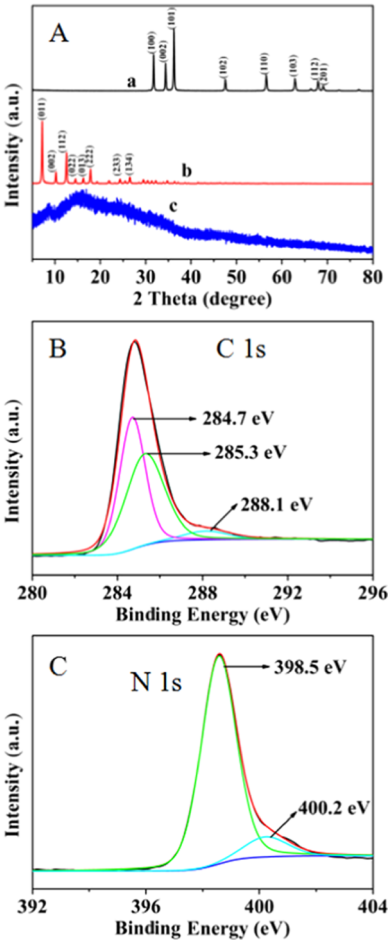

Figure 2. (A) PXRD patterns of ZnO nanorods (a), ZIF-8 nanopolyhedra (b), and NPC-ZnO nanopolyhedra (c). (B) C 1s and (C) N 1s XPS spectra of NPC-ZnO nanopolyhedra.

In Figure 2A, the X-ray diffraction (XRD) patterns of the ZnO nanorods (curve a) and ZIF-8 nanopolyhedra (curve b) are matched well with the standard card of ZnO (JCPDS No. 36-1451) and the previous reported XRD results of ZIF-8, respectively.[40,54] However, for the NPC-ZnO nanopolyhedra, the typical peaks of ZIF-8 disappear, implying that the crystalline structure of ZIF-8 is destroyed completely during the heat treatment at 600 °C. The related XRD pattern (curve c) further indicates that the nitrogen-doped porous carbon in the NPC-ZnO nanopolyhedra has a low graphitization degree due to the low-temperature treatment (600 °C).[55] Although no obvious peaks of ZnO can be observed in curve c (Figure 2A), Zn element in ZIF-8 should be changed to ZnO after the heat treatment at 600 °C, as reported previously and confirmed by the EDS results (Figure 1D). (When the temperature is higher than 800 °C, ZnO is reduced to Zn metal. Zn metal will be evaporated when the temperature is further increased and higher than 904 °C (boiling point of Zn, 904 °C).[56,57]) These results are further confirmed by the high-resolution TEM (HRTEM) images (Figure S1) at the bulk and the edge of NPC-ZnO nanopolyhedra and the related Raman spectroscopic pattern (Figure S2). It is noted that no lattice planes can be observed obviously for carbons and ZnO in Figure S1, and

DOI: 10.1021/acsami.7b10856
ACS Appl. Mater. Interfaces 2017, 9, 42482−42491

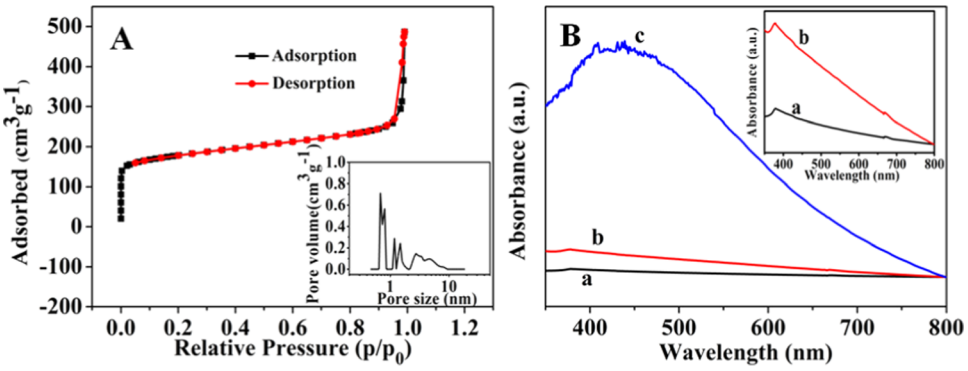

Figure 3. (A) Nitrogen adsorption−desorption isotherms of the NPC-ZnO nanopolyhedra at 77 K. Inset plot is the corresponding pore size distribution of the NPC-ZnO nanopolyhedra. (B) UV−vis absorption spectra of ZnO nanorods (a), ZIF-8 nanopolyhedra (b), and NPC-ZnO nanopolyhedra (c).

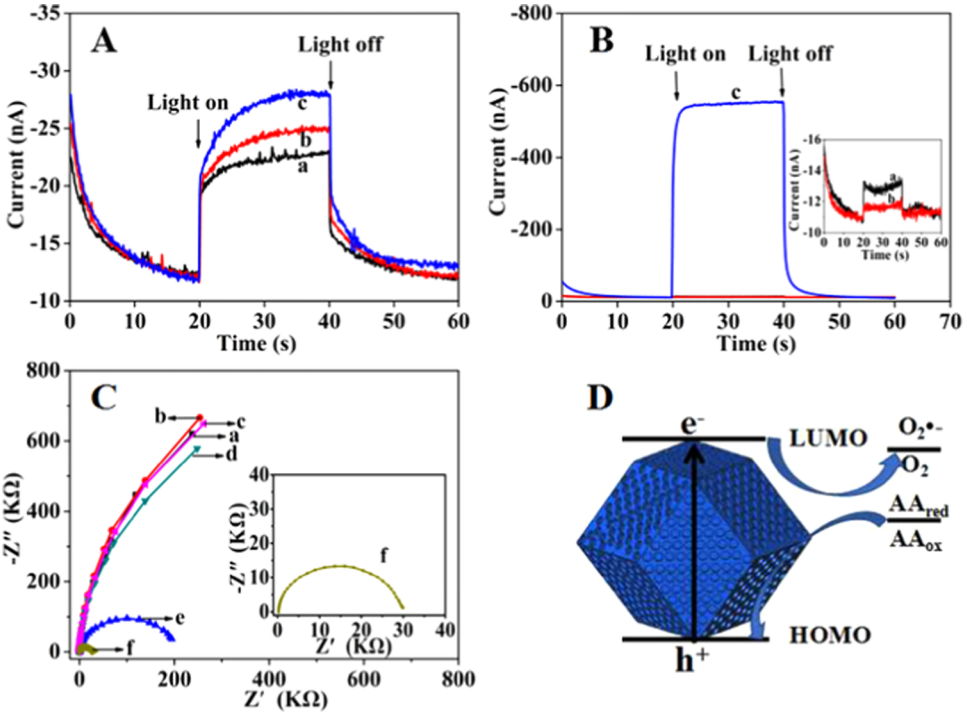

Figure 4. (A) Photocurrent responses of the ITO/NPC-ZnO electrode in the N_2-saturated (a), air-saturated (b), and O_2-saturated (c) 0.1 M Tris−HCl (pH 8.0) buffer solution. (B) Photocurrent responses of ITO/ZnO (a), ITO/ZIF-8 (b), and ITO/NPC-ZnO (c) electrodes in 0.1 M Tris−HCl (pH 8.0) containing 1 mM AA. (C) Nyquist plots of ITO/ZnO (a, d), ITO/ZIF-8 (b, c), and ITO/NPC-ZnO (e, f) electrodes in 0.1 M Tris−HCl (pH 8.0) buffer solutions containing 1 mM AA at −0.2 V in the frequency range of 0.1 Hz to 100 kHz with an amplitude of 5 mV ((a, b, e) without illumination, (c, d, f) with illumination (λ > 420 nm)). (D) The cathodic photocurrent generation mechanism of the ITO/NPC-ZnO electrode. PEC tests were performed at −0.3 V under light excitation (λ > 420 nm).

there is a high area ratio (1.03) of Raman bands of disordered graphite (D band) and graphite (G band) in Figure S2.

To further explore the elemental compositions and chemical states of the NPC-ZnO nanopolyhedra, the XPS investigation was carried out. From Figure S3A, it is clear that the four elements (C, N, O, and Zn) exist in the sample, which is in agreement with the EDS results (Figure 1D). From Figure 2B, the C 1s spectrum of the NPC-ZnO nanopolyhedra can be deconvoluted into three peaks at 284.7, 285.3, and 288.1 eV, which are associated with C sp^3−C sp^3, C sp^2−C sp^2, and C═N, respectively.[58] Similarly, the N 1s spectrum of the NPC-ZnO nanopolyhedra can be mainly deconvoluted into two peaks centered at about 398.5 and 400.2 eV, which are assignable to pyridinic N and pyrrolic N, respectively (Figure 2C).[59] Further quantitative analysis of the N 1s spectrum indicates that the majority of N in NPC-ZnO nanopolyhedra is pyridinic N (89.3%), which has a lone pair of electrons, promoting the electron transfer.[59] These may provide an additional merit of the NPC-ZnO nanopolyhedra in the construction of PEC biosensors. On the other hand, the two peaks centered at about 530.8 and 531.7 eV in the O 1s spectrum of the NPC-ZnO nanopolyhedra (Figure S3B) belong to the O^{2-} ions and the oxygen vacancy on the surface of materials, respectively.[60] The Zn 2p spectrum of the NPC-ZnO nanopolyhedra includes two peaks at about 1021.6 and 1044.7 eV, assigned to Zn $2p_{3/2}$ and $2p_{1/2}$, respectively (Figure S3C). This suggests that Zn^{2+} ions exist in the NPC-ZnO nanopolyhedra based on the distance (23.1 eV) between the

DOI: 10.1021/acsami.7b10856
ACS Appl. Mater. Interfaces 2017, 9, 42482−42491

two peaks.[61] According to the XPS results, NPC-ZnO nanopolyhedra are the N-doped carbon-ZnO composites.

To further explore the porosity, the N_2 adsorption−desorption isotherms of the NPC-ZnO nanopolyhedra were determined, and are shown in Figure 3A. The Brunauer−Emmett−Teller specific surface area (SSA) of the NPC-ZnO nanopolyhedra is calculated to be 609.2 m^2 g^{-1}. Additionally, from the inset of Figure 3A, the corresponding Barrett−Joyner−Halenda pore size distribution curve indicates that the NPC-ZnO nanopolyhedra contain mainly two types of pores: micropores (<2 nm) and mesopores (2−8 nm). The average pore size of mesopores is 3.0 nm, which is beneficial to quick mass transfer of molecules and ion diffusion (such as AA).[62] On the basis of the high specific surface area and the synergic effects of various pores with different sizes, the NPC-ZnO nanopolyhedra are expected to possess good photoelectrochemical properties.

To investigate the spectroscopic properties of the NPC-ZnO nanopolyhedra, the UV−vis absorption spectra of different materials are measured (Figure 3B). The ZnO nanorods show a characteristic peak at 380 nm according to its band gap (curve a), whereas the ZIF-8 nanopolyhedra show the similar absorption peak to ZnO nanorods (curve b). However, the maximum absorption band of the NPC-ZnO nanopolyhedra appears at 439 nm, which is red-shifted obviously in comparison with that of ZnO nanorod and the ZIF-8 nanopolyhedra, the 60 nm red-shift could be attributed to the interaction between NPC and ZnO. The obviously enhanced visible absorption intensity and a broad absorption range of the NPC-ZnO nanopolyhedra indicate their suitability to be photoactive materials under visible-light (λ > 420 nm) irradiation, which is beneficial to the construction of PEC biosensors.

3.2. PEC Properties of the ITO/NPC-ZnO Electrode. Figure 4A shows the effect of the dissolved oxygen on the photocurrent of ITO/NPC-ZnO electrode. It is noted that the photocurrent increases slightly with the increase in illumination time due to the possible reason that the diffusion rate of the dissolved oxygen from the electrolyte solution to the electrode surface is faster than the reduction rate of oxygen on the electrode surface. On the other hand, in the N_2-saturated electrolyte solution (curve a), a slight photocurrent of the ITO/NPC-ZnO electrode is observed. With the increase in dissolved oxygen concentration (from oxygen in air to pure oxygen), the photocurrent increases (curves b and c). The increased photocurrent of the ITO/NPC-ZnO electrode may be attributed to the fact that the dissolved oxygen accepts electrons from the NPC-ZnO nanopolyhedra-based PEC system. As is known, a suitable electron acceptor can scavenge the photogenerated electrons and greatly enhance the charge separation of semiconductors, resulting in promoted photocurrent.[63]

It is worth noting that electron donors with suitable energy level can enhance photocurrent via being oxidized by photogenerated holes.[64,65] Furthermore, AA is widely chosen as the electron donor for the PEC investigations. As shown in Figure 4B, under light irradiation, the introduction of AA to the electrolyte solution leads to an obvious increase in the photocurrent of the ITO/NPC-ZnO electrode (curve c), demonstrating that AA can effectively be oxidized by photogenerated holes on the valence band (highest occupied molecular orbital (HOMO)) of the NPC-ZnO nanopolyhedra to reduce the recombination of photogenerated electron−hole pairs, resulting in the enhanced photocurrent. In addition, the photocurrent of NPC-ZnO nanopolyhedra is around 500× higher than that of ZnO nanorod and ZIF-8 nanopolyhedra, confirming that the PEC activity can be greatly enhanced by interaction between the NPC and highly dispersed ZnO in the NPC-ZnO nanopolyhedra. This should be attributed to the change in the band gap of ZnO by nitrogen-doped carbons and the enrichment of dissolved oxygen and AA in the frameworks of the NPC-ZnO nanopolyhedra due to their high surface area and porous structure.

On the other hand, to further verify the PEC behaviors of the NPC-ZnO nanopolyhedra, different modified ITO electrodes are characterized by electrochemical impedance spectroscopy with or without illumination, and the corresponding results are shown in Figure 4C. The semicircle diameter at a higher frequency range is proportional to the interfacial charge-transfer resistance (R_{ct}) of the electrode.[66] From Figure 4C, the order of the R_{ct} values of different electrodes is as follows: (1) without illumination, ITO/NPC-ZnO (211 ± 3.6 kΩ) < ITO/ZnO (2754 ± 39.7 kΩ) < ITO/ZIF-8 (3002 ± 35.2 kΩ); and (2) with illumination, ITO/NPC-ZnO (28 ± 0.6 kΩ) < ITO/ZnO (2447 ± 43.5 kΩ) < ITO/ZIF-8 (2730 ± 38.1 kΩ). It is noted that the samples have lower R_{ct} values with illumination than without illumination, and the R_{ct} value of the ITO/NPC-ZnO electrode is much lower than that of the ITO/ZnO and ITO/ZIF-8 electrodes either with or without illumination. The possible reasons may be as follows: (1) the electrical conductivity of the ITO/NPC-ZnO electrode is higher than that of the ITO/ZnO and ITO/ZIF-8 electrodes due to the good electrical conductivity of NPC and poor electrical conductivity of ZnO and ZIF-8. (2) As reported in the previous papers,[29,38] the illumination would decrease the R_{ct} value of the photoelectrode due to the photoelectric effect of semiconductor. Here, based on the results shown in Figure 4C, the ITO/NPC-ZnO electrode has better photoelectric properties than ITO/ZnO and ITO/ZIF-8 electrodes under light excitation (λ > 420 nm). These correspond with the observations from Figure 4B and clearly indicate that NPC-ZnO nanopolyhedra have excellent PEC behavior and should be suitable for the construction of PEC sensors.

Based on the above results, the photocurrent generation mechanism of the NPC-ZnO nanopolyhedra in 0.1 M Tris−HCl (pH 8.0) aqueous solution containing dissolved oxygen and AA is proposed and illustrated in Figure 4D. Due to their good visible absorption property (Figure 3B) and low interfacial charge-transfer resistance (R_{ct}) (Figure 4C), the NPC-ZnO nanopolyhedra show good photoelectrical properties under visible-light (λ > 420 nm) irradiation. When the NPC-ZnO nanopolyhedra are excited by visible light, electrons/holes are formed on the conduction band (lowest unoccupied molecular orbital (LUMO))/valence band (HOMO), respectively. Then, parts of photogenerated electron−hole pairs recombine and parts of the photogenerated electrons transfer from the LUMO of NPC-ZnO nanopolyhedra to O_2 (electron acceptor) in the electrolyte for the electrochemical reduction of O_2. When the electrolyte solution contains AA (electron donor), photogenerated holes can effectively oxidize AA and the recombination of photogenerated electron−hole pairs is reduced, resulting in the enhanced cathodic photocurrent.[38]

3.3. Feasibility of the NPC-ZnO Nanopolyhedra for ALP Assay. To further explore the application of NPC-ZnO nanopolyhedra in PEC biosensors, a ITO/NPC-ZnO/ALP

DOI: 10.1021/acsami.7b10856
ACS Appl. Mater. Interfaces 2017, 9, 42482−42491

electrode was fabricated by simply adding ALP to the ITO/NPC-ZnO electrode, and the catalytic properties of ALP toward the hydrolyzation of AAP were investigated by the PEC method. From Figure 5, it is noted obviously that no photocurrent appears on the bare ITO electrode (curve a). After the modification of the ITO electrode with NPC-ZnO nanopolyhedra, a small photocurrent can be observed (curve b) due to the dissolved oxygen as the electron acceptor. However, for the ITO/NPC-ZnO/ALP electrode, an obvious photocurrent response can be observed (curve c). This should be attributed to the hydrolyzation of AAP by ALP enzyme to produce AA, and AA acts as an electron donor to be oxidized by photogenerated holes and to enhance greatly the photocurrent.[20] These results clearly indicate that the NPC-ZnO nanopolyhedra-based PEC biosensor can provide a new platform for ALP assay. On the other hand, the photocurrent decays with the increase in the illumination time due to the consumption of AA. Thus, the maximum photocurrent value is used for the following quantitative analysis of ALP.

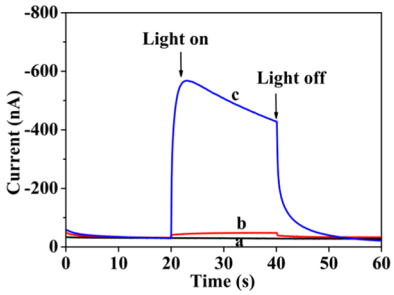

Figure 5. Photocurrent responses of different modified electrodes: ITO (a), ITO/NPC-ZnO (b), and ITO/NPC-ZnO/ALP (c). The added concentration of ALP, 1000 U L^{-1}; PEC tests were performed at −0.3 V in 0.1 M Tris−HCl buffer (pH 8.0) containing 1.2 mM AAP under light excitation (λ > 420 nm).

3.4. Optimization of Experimental Conditions. To achieve excellent performance of the ITO/NPC-ZnO electrode for ALP assay, several experiment parameters, including the applied potential, the adsorption time of ALP on the ITO/NPC-ZnO electrode, the reaction time between ALP and AAP, and AAP concentration, were optimized.

The applied potential is a critical parameter in the PEC sensor and optimized in this work. As shown in Figure 6A, it is noted that the photocurrent increases when the applied potential shifts negatively. Considering the changed tendency of photocurrent and the bad effects of the high applied potential (either anodic or cathodic potential) on the biomolecules and the surface state of the photoelectrodes,[67] −0.3 V is selected as the optimal applied potential to obtain large cathodic photocurrent.

In this work, AA, generated from the hydrolyzation of AAP by ALP, is used as the electron donor to increase the photocurrent. Thus, the adsorption time of ALP on the ITO/NPC-ZnO electrode is a key parameter and should be optimized. As shown in Figure 6B, the photocurrent of the ITO/NPC-ZnO/ALP electrode increases with the increase in the ALP adsorption time, and then gradually reaches a plateau. This can be explained as follows: with the increase in the ALP adsorption time, the amount of ALP adsorbed on the ITO/

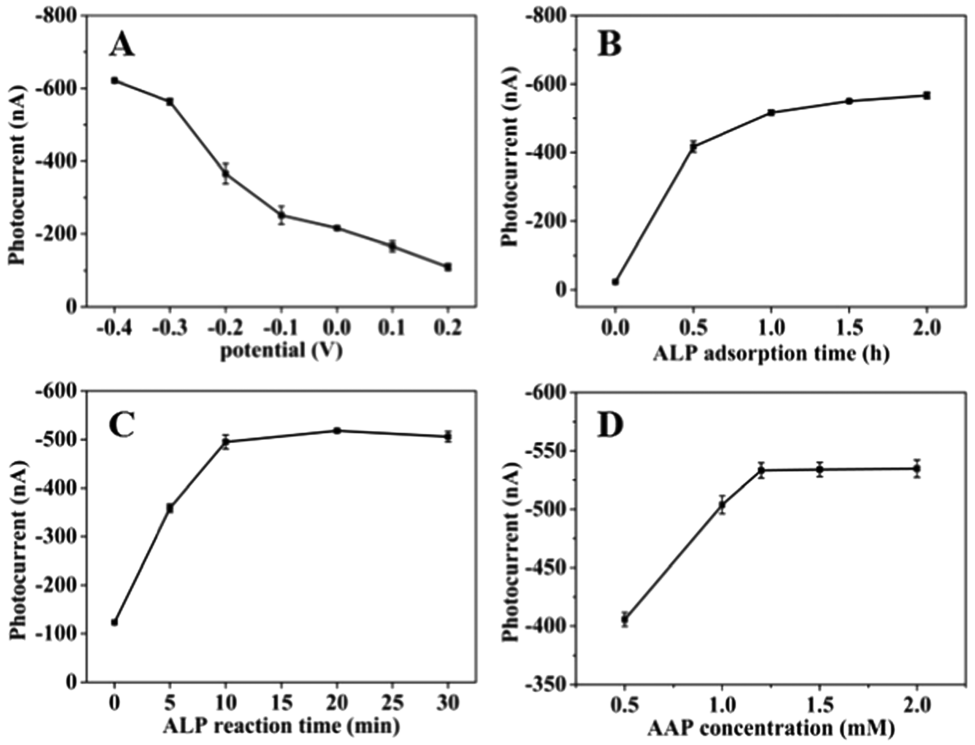

Figure 6. (A) Effect of applied potential on the photocurrent response of the ITO/NPC-ZnO electrode in 0.1 M Tris−HCl (pH 8.0) containing 1 mM AA. (B−D) The effects of different parameters on the photocurrent responses of the ITO/NPC-ZnO/ALP electrode, (B) adsorption time of ALP (the added concentration of ALP, 1000 U L^{-1}; reaction time between ALP and AAP, 30 min; AAP concentration, 1.2 mM); (C) reaction time between ALP and AAP (the added concentration of ALP, 1000 U L^{-1}; adsorption time of ALP, 1 h; AAP concentration, 1.2 mM); (D) concentration of AAP (the added concentration of ALP, 1000 U L^{-1}; adsorption time of ALP, 1 h; reaction time between ALP and AAP, 20 min).

DOI: 10.1021/acsami.7b10856
ACS Appl. Mater. Interfaces 2017, 9, 42482−42491

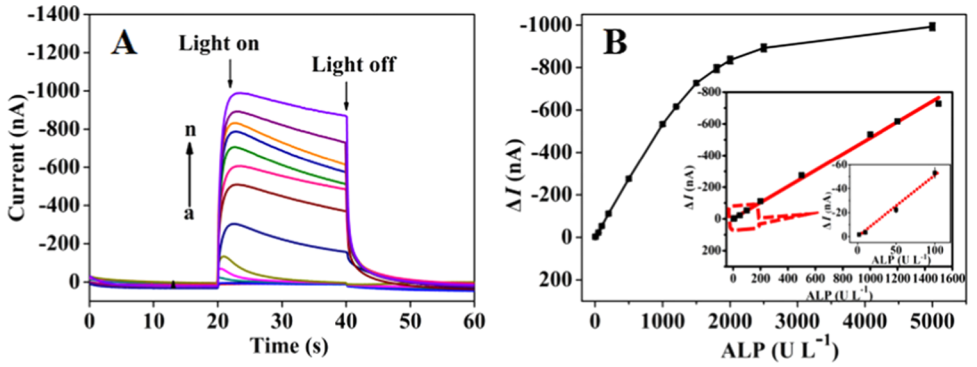

Figure 7. (A) Photocurrent responses of the ITO/NPC-ZnO/ALP electrode to the different added concentrations of ALP. The concentrations are (from a to n) 0, 2, 10, 50, 100, 200, 500, 1000, 1200, 1500, 1800, 2000, 2500, and 5000 U L^{-1}. (B) Dependence of ΔI on the added ALP concentration. Inset shows the linear fit plots of ΔI as a function of the added ALP concentration.

NPC-ZnO/ALP electrode increases, and then a saturation of adsorption of ALP is reached. From Figure 6B, 1 h is selected as the optimal ALP adsorption time.

On the other hand, the reaction time between ALP and AAP is optimized. Figure 6C shows that the photocurrent increases with the increase in the reaction time and then reaches a plateau at 10 min. To ensure sufficient reaction time, 20 min is taken as the optimal reaction time between ALP and AAP.

The effect of AAP concentration on the photocurrent response of the ITO/NPC-ZnO/ALP electrode has also been investigated. Figure 6D shows that the photocurrent of the electrode increases with the increase in AAP concentration. When the concentration of AAP is more than 1.2 mM, a plateau can be found due to the saturation effect of the activity and concentration of ALP on the electrode. Thus, 1.2 mM is selected as the optimal concentration of AAP.

3.5. PEC Assay of ALP. Under optimal conditions, the analytical performance of the proposed NPC-ZnO nanopolyhedra-based PEC electrode was examined for various concentrations of ALP. As shown in Figure 7A, it is noted that the photocurrent increases with increase in the ALP concentration. Figure 7B shows the corresponding calibration curve ($\Delta I = I - I_0$, where I and I_0 represent the photocurrents of the electrode in the presence and absence of ALP, respectively). It is noted that the value of ΔI is linear with the ALP concentration in the range from 2 to 1500 U L^{-1}, with the detection limit of 1.7 U L^{-1} (3σ), and the linear regression equation is ΔI (nA) = 1.02 − 0.51C_{ALP} (U L^{-1}) (R^2 = 0.9988). As shown in Table 1, the NPC-ZnO nanopolyhedra-based PEC biosensor for ALP assay exhibits a lower detection limit and a wider linear range than most of the reported methods, implying that the developed NPC-ZnO nanopolyhedra have great potential for the construction of ALP-based PEC biosensors.

Table 1. Comparison of Some Methods for ALP Assay[a]

analysis methods	detection limit (U L^{-1})	linear range (U L^{-1})	ref
fluorescence	5	30−240	46
	10	25−200	68
	18	18−100	47
electrochemiluminescence	2	2−25	49
	2	6−600	50
colorimetry	3.3	5−100	51
	10	10−600	52
	32	32−200	69
photoelectrochemistry	1.7	2−1500	this work

[a]One unit of ALP is defined as the amount of the enzyme that hydrolyzes 1.0 μmol of *p*-nitrophenyl phosphate per minute at 37 °C.

3.6. Selectivity, Reproducibility, and Stability of the PEC Biosensor. Taking four proteins, including pepsin, lysozyme, GO_X and bovine serum albumin (BSA), as interferents, the selectivity of the proposed PEC method was investigated. The solutions containing pure ALP, pure interferents, and the mixture of ALP with four interferents were added to the ITO/NPC-ZnO electrodes and then the photocurrents of the electrodes were measured in 0.1 M Tris−HCl (pH 8.0) containing 1.2 mM AAP. According to the normal concentration of ALP in adults (46−190 U L^{-1}),[70] 100 U L^{-1} (3.3×10^{-5} mg mL^{-1}) of ALP is used here and the concentrations of the interfering proteins (0.1 mg mL^{-1}) are much higher than that of ALP. As shown in Figure 8A, it is noted that no significant photocurrent is observed when the ITO/NPC-ZnO electrode is incubated with pure interfering protein solution. However, the photocurrent can be observed obviously when the ITO/NPC-ZnO electrode is incubated with pure ALP. This can be ascribed to the fact that ALP can only enzymatically hydrolyze AAP to produce AA (electron donor). Also, the photocurrent for the mixed solution of ALP and interferents is about 90.3% of that obtained in the pure ALP sample with the same concentration of ALP. These results clearly indicate that the developed method possesses acceptable selectivity. The reproducibility of the developed assay system is also evaluated. For 1000 U L^{-1} ALP, the relative standard deviation of 6.3% is obtained for five ITO/NPC-ZnO/ALP electrodes. This demonstrates the satisfactory reproducibility of the ITO/NPC-ZnO/ALP electrode. Additionally, the stability of the ITO/NPC-ZnO/ALP electrode is further investigated. Three independent experiments demonstrate that the photocurrent of the ITO/NPC-ZnO/ALP electrode does not change significantly after its storage in a refrigerator at 4 °C over 2 weeks. These results indicate that the ITO/NPC-ZnO/ALP electrode has acceptable stability.

3.7. Recovery Test. To further evaluate the practical application in a complex system, the developed PEC electrode was carried out to detect ALP in normal human serum samples without active ALP. The 50-fold diluted human serum solutions (diluted with 1× CutSmart buffer) were spiked with different concentrations of ALP (100, 500, and 1000 U L^{-1}). As shown in Figure 8B, the photocurrent responses to ALP in human serum samples were almost the same with that in 1× CutSmart

DOI: 10.1021/acsami.7b10856
ACS Appl. Mater. Interfaces 2017, 9, 42482−42491

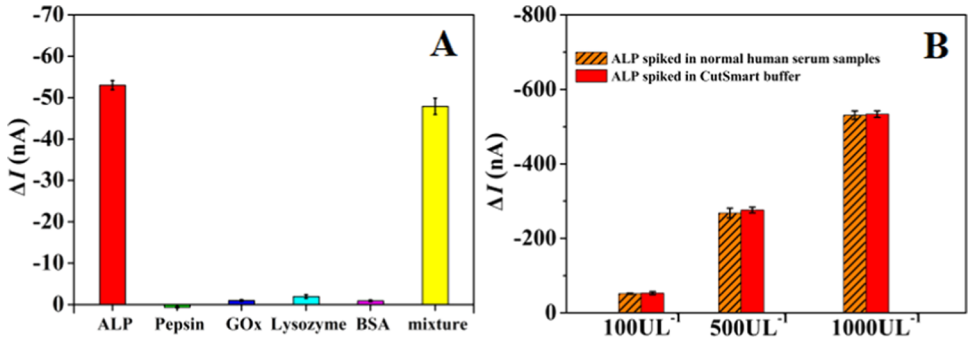

Figure 8. (A) Selectivity of the PEC biosensor for ALP detection. The added concentration of ALP, 100 U L^{-1} (3.3×10^{-5} mg mL^{-1}); the added concentration of other protein (pepsin or lysozyme, GO_X and BSA), 0.1 mg mL^{-1}, and the mixture of ALP (3.3×10^{-5} mg mL^{-1}) and these four proteins (the concentration of each protein, 0.025 mg mL^{-1}). (B) Comparison of the ALP assay in 1× CutSmart buffer and human serum samples. The added concentration of ALP, 100, 500, and 1000 U L^{-1}; AAP concentration, 1.2 mM.

buffer, and the recoveries in human serum samples for the added ALP with 100, 500, and 1000 U L^{-1} are 97.2, 97.1, and 99.5%, respectively. These results clearly reveal that the recovery of the developed NPC-ZnO-based PEC sensor is satisfactory and has great potential applications in ALP practical analysis.

4. CONCLUSIONS

By direct carbonization of the ZIF-8 nanopolyhedra in a nitrogen atmosphere, novel photoactive materials, NPC-ZnO nanopolyhedra with rhombic dodecahedron morphology, were prepared. The obtained NPC-ZnO nanopolyhedra have uniform particle size of about 100 nm, high specific surface area of 609.2 m^2 g^{-1}, and excellent photoelectrochemical properties in the aqueous media with dissolved oxygen and AA. Taking ALP as a model, the ITO/NPC-ZnO electrode was shown to have excellent analytical performance for ALP assay with a wide linear response range from 2 to 1500 U L^{-1} and a low detection limit of 1.7 U L^{-1}. Moreover, the PEC sensor possesses acceptable selectivity, reproducibility, and stability. The prepared NPC-ZnO nanopolyhedra provide a new photoactive material for the construction of PEC sensors and may have promising applications in PEC assay of heavy metal ions, organic pollutants, and biomolecules.

■ ASSOCIATED CONTENT

Supporting Information

The Supporting Information is available free of charge on the ACS Publications website at DOI: 10.1021/acsami.7b10856.

HRTEM images and Raman spectrum of the NPC-ZnO nanopolyhedra, XPS survey spectrum of the NPC-ZnO nanopolyhedra, and the related high-resolution spectra of O 1s and Zn 2p (PDF)

■ AUTHOR INFORMATION

Corresponding Author

*E-mail: chenjinhua@hnu.edu.cn. Tel: +86-731-88821848.

ORCID

Jinhua Chen: 0000-0001-5089-0927

Notes

The authors declare no competing financial interest.

■ ACKNOWLEDGMENTS

This work was financially supported by NSFC (21475035, 21235002, and 21727810), the Foundation for Innovative Research Groups of NSFC (21521063), and PCSIRT (IRT1238).

■ REFERENCES

(1) Mei, L.-P.; Liu, F.; Pan, J.-B.; Zhao, W.-W.; Xu, J.-J.; Chen, H.-Y. Enediol-Ligands-Encapsulated Liposomes Enables Sensitive Immunoassay: A Proof-of-Concept for General Liposomes-Based Photoelectrochemical Bioanalysis. *Anal. Chem.* **2017**, *89*, 6300−6304.

(2) Liu, Q.; Huan, J.; Hao, N.; Qian, J.; Mao, H.; Wang, K. Engineering of Heterojunction-Mediated Biointerface for Photoelectrochemical Aptasensing: Case of Direct Z-Scheme CdTe−Bi_2S_3 Heterojunction with Improved Visible-Light-Driven Photoelectrical Conversion Efficiency. *ACS Appl. Mater. Interfaces* **2017**, *9*, 18369−18376.

(3) Li, C.; Wang, H.; Shen, J.; Tang, B. Cyclometalated Iridium Complex-Based Label-Free Photoelectrochemical Biosensor for DNA Detection by Hybridization Chain Reaction Amplification. *Anal. Chem.* **2015**, *87*, 4283−4291.

(4) Wang, L.; Ma, W.; Gan, S.; Han, D.; Zhang, Q.; Niu, L. Engineered Photoelectrochemical Platform for Rational Global Antioxidant Capacity Evaluation Based on Ultrasensitive Sulfonated Graphene−TiO_2 Nanohybrid. *Anal. Chem.* **2014**, *86*, 10171−10178.

(5) Zhao, W.-W.; Wang, J.; Zhu, Y.-C.; Xu, J.-J.; Chen, H.-Y. Quantum Dots: Electrochemiluminescent and Photoelectrochemical Bioanalysis. *Anal. Chem.* **2015**, *87*, 9520−9531.

(6) Wang, K.; Zhang, R.; Sun, N.; Li, X.; Wang, J.; Cao, Y.; Pei, R. Near-Infrared Light-Driven Photoelectrochemical Aptasensor Based on the Upconversion Nanoparticles and TiO_2/CdTe Heterostructure for Detection of Cancer Cells. *ACS Appl. Mater. Interfaces* **2016**, *8*, 25834−25839.

(7) Wang, J.; Liu, ZH.; Hu, C.; Hu, S. Ultrasensitive Photoelectrochemical Biosensing of Multiple Biomarkers on a Single Electrode by a Light Addressing Strategy. *Anal. Chem.* **2015**, *87*, 9368−9375.

(8) Li, Z.; Xin, Y.; Zhang, Z. New Photocathodic Analysis Platform with Quasi-Core/Shell Structured TiO_2@Cu_2O for Sensitive Detection of H_2O_2 Release from Living Cells. *Anal. Chem.* **2015**, *87*, 10491−10497.

(9) Fan, G.-C.; Han, L.; Zhang, J.-R.; Zhu, J.-J. Enhanced Photoelectrochemical Strategy for Ultrasensitive DNA Detection Based on Two Different Sizes of CdTe Quantum Dots Cosensitized TiO_2/CdS:Mn Hybrid Structure. *Anal. Chem.* **2014**, *86*, 10877−10884.

(10) Zang, Y.; Lei, J.; Ling, P.; Ju, H. Catalytic Hairpin Assembly-Programmed Porphyrin−DNA Complex as Photoelectrochemical Initiator for DNA Biosensing. *Anal. Chem.* **2015**, *87*, 5430−5436.

(11) Liang, M.; Liu, S.; Wei, M.; Guo, L.-H. Photoelectrochemical Oxidation of DNA by Ruthenium Tris(bipyridine) on a Tin Oxide Nanoparticle Electrode. *Anal. Chem.* **2006**, *78*, 621−623.

(12) Shen, Q.; Han, L.; Fan, G.; Zhang, J.-R.; Jiang, L.; Zhu, J.-J. "Signal-on" Photoelectrochemical Biosensor for Sensitive Detection of

DOI: 10.1021/acsami.7b10856
ACS Appl. Mater. Interfaces 2017, 9, 42482−42491

Human T-Cell Lymphotropic Virus Type II DNA: Dual Signal Amplification Strategy Integrating Enzymatic Amplification with Terminal Deoxynucleotidyl Transferase-Mediated Extension. *Anal. Chem.* **2015**, *87*, 4949−4956.
(13) Wang, G.-L.; Xu, J.-J.; Chen, H.-Y.; Fu, S.-Z. Label-Free Photoelectrochemical Immunoassay for α-Fetoprotein Detection Based on TiO_2/CdS Hybrid. *Biosens. Bioelectron.* **2009**, *25*, 791−796.
(14) Ge, L.; Wang, P.; Ge, S.; Li, N.; Yu, J.; Yan, M.; Huang, J. Photoelectrochemical Lab-on-Paper Device Based on an Integrated Paper Supercapacitor and Internal Light Source. *Anal. Chem.* **2013**, *85*, 3961−3970.
(15) Zhuang, J.; Tang, D.; Lai, W.; Xu, M.; Tang, D. Target-Induced Nano-Enzyme Reactor Mediated Hole-Trapping for High-Throughput Immunoassay Based on a Split-Type Photoelectrochemical Detection Strategy. *Anal. Chem.* **2015**, *87*, 9473−9480.
(16) Zang, Y.; Lei, J.; Zhang, L.; Ju, H. In Situ Generation of Electron Acceptor for Photoelectrochemical Biosensing via Hemin-Mediated Catalytic Reaction. *Anal. Chem.* **2014**, *86*, 12362−12368.
(17) Li, M.; Zheng, Y.; Liang, W.; Yuan, Y.; Chai, Y.; Yuan, R. An Ultrasensitive "on−off−on" Photoelectrochemical Aptasensor Based on Signal Amplification of Fullerene/CdTe Quantum Dots Sensitized Structure and Efficient Quenching with Manganese Porphyrin. *Chem. Commun.* **2016**, *52*, 8138−8141.
(18) Ma, Z.-Y.; Ruan, Y.-F.; Xu, F.; Zhao, W.-W.; Xu, J.-J.; Chen, H.-Y. Protein Binding Bends the Gold Nanoparticle Capped DNA Sequence: Toward Novel Energy-Transfer-Based Photoelectrochemical Protein Detection. *Anal. Chem.* **2016**, *88*, 3864−3871.
(19) Ma, Z.-Y.; Xu, F.; Qin, Y.; Zhao, W.-W.; Xu, J.-J.; Chen, H.-Y. Invoking Direct Exciton−Plasmon Interactions by Catalytic Ag Deposition on Au Nanoparticles: Photoelectrochemical Bioanalysis with High Efficiency. *Anal. Chem.* **2016**, *88*, 4183−4187.
(20) Shen, Q.; Zhao, X.; Zhou, S.; Hou, W.; Zhu, J.-J. ZnO/CdS Hierarchical Nanospheres for Photoelectrochemical Sensing of Cu^{2+}. *J. Phys. Chem. C* **2011**, *115*, 17958−17964.
(21) Yan, Z.; Wang, Z.; Miao, Z.; Liu, Y. Dye-Sensitized and Localized Surface Plasmon Resonance Enhanced Visible-Light Photoelectrochemical Biosensors for Highly Sensitive Analysis of Protein Kinase Activity. *Anal. Chem.* **2016**, *88*, 922−929.
(22) Hayashi, H.; Lightcap, I. V.; Tsujimoto, M.; Takano, M.; Umeyama, T.; Kamat, P. V.; Imahori, H. Electron Transfer Cascade by Organic/Inorganic Ternary Composites of Porphyrin, Zinc Oxide Nanoparticles, and Reduced Graphene Oxide on a Tin Oxide Electrode that Exhibits Efficient Photocurrent Generation. *J. Am. Chem. Soc.* **2011**, *133*, 7684−7687.
(23) Zhuang, J.; Lai, W.; Xu, M.; Zhou, Q.; Tang, D. Plasmonic AuNP/G-C_3N_4 Nanohybrid-Based Photoelectrochemical Sensing Platform for Ultrasensitive Monitoring of Polynucleotide Kinase Activity Accompanying DNAzyme-Catalyzed Precipitation Amplification. *ACS Appl. Mater. Interfaces* **2015**, *7*, 8330−8338.
(24) Wang, Y.; Wang, W.; Wang, S.; Chu, W.; Wei, T.; Tao, H.; Zhang, C.; Sun, Y. Enhanced Photoelectrochemical Detection of L-Cysteine Based on the Ultrathin Polythiophene Layer Sensitized Anatase TiO_2 on F-Doped Tin Oxide Substrates. *Sens. Actuators, B* **2016**, *232*, 448−453.
(25) Liu, Y.; Yan, K.; Zhang, J. Graphitic Carbon Nitride Sensitized with CdS Quantum Dots for Visible-Light-Driven Photoelectrochemical Aptasensing of Tetracycline. *ACS Appl. Mater. Interfaces* **2016**, *8*, 28255−28264.
(26) Fan, D.; Guo, C.; Ma, H.; Zhao, D.; Li, Y.; Wu, D.; Wei, Q. Facile Fabrication of an Aptasensor for Thrombin Based on Graphitic Carbon Nitride/TiO_2 with High Visible-Light Photoelectrochemical Activity. *Biosens. Bioelectron.* **2016**, *75*, 116−122.
(27) Yan, K.; Liu, Y.; Yang, Y.; Zhang, J. A Cathodic "Signal-off" Photoelectrochemical Aptasensor for Ultrasensitive and Selective Detection of Oxytetracycline. *Anal. Chem.* **2015**, *87*, 12215−12220.
(28) Sun, B.; Dong, J.; Shi, W.-J.; Ai, S.-Y. A Hierarchical Charge Transport Cascade Based on W-Bi_2S_3/Poly(Thiophenyl-3-Boronic Acid) Hybrid for Robust Photoelectrochemical Analysis of Subgroup J of Avian Leukosis Virus. *Sens. Actuators, B* **2016**, *229*, 75−81.
(29) Zhao, K.; Yan, X.; Gu, Y.; Kang, Z.; Bai, Z.; Cao, S.; Liu, Y.; Zhang, X.; Zhang, Y. Self-Powered Photoelectrochemical Biosensor Based on CdS/RGO/ZnO Nanowire Array Heterostructure. *Small* **2016**, *12*, 245−251.
(30) Hu, C.; Zheng, J.; Su, X.; Wang, J.; Wu, W.; Hu, S. Ultrasensitive All-Carbon Photoelectrochemical Bioprobes for Zeptomole Immunosensing of Tumor Markers by an Inexpensive Visible Laser Light. *Anal. Chem.* **2013**, *85*, 10612−10619.
(31) Wang, K.; Sun, N.; Li, X.; Zhang, R.; Zu, G.; Wang, J.; Pei, R. A Hemin Binding G-Quadruplex/Pb^{2+} Complex to Construct a Visible Light Activated Photoelectrochemical Sensor on a ZnO/BiOI Heterostructure. *Anal. Methods* **2015**, *7*, 9340−9346.
(32) Musselman, K. P.; Marin, A.; Wisnet, A.; Scheu, C.; MacManus-Driscoll, J. L.; Schmidt-Mende, L. A Novel Buffering Technique for Aqueous Processing of Zinc Oxide Nanostructures and Interfaces, and Corresponding Improvement of Electrodeposited ZnO−Cu_2O Photovoltaics. *Adv. Funct. Mater.* **2011**, *21*, 573−582.
(33) Lu, S.; Qi, J.; Liu, S.; Zhang, Z.; Wang, Z.; Lin, P.; Liao, Q.; Liang, Q.; Zhang, Y. Piezotronic Interface Engineering on ZnO/Au-Based Schottky Junction for Enhanced Photoresponse of a Flexible Self-Powered UV Detector. *ACS Appl. Mater. Interfaces* **2014**, *6*, 14116−14122.
(34) Shen, K.; Chen, X.; Chen, J.; Li, Y. Development of MOF-Derived Carbon-Based Nanomaterials for Efficient Catalysis. *ACS Catal.* **2016**, *6*, 5887−5903.
(35) Liu, T.-Z.; Hu, R.; Zhang, X.; Zhang, K.-L.; Liu, Y.; Zhang, X.-B.; Bai, R.-Y.; Li, D.; Yang, Y.-H. Metal−Organic Framework Nanomaterials as Novel Signal Probes for Electron Transfer Mediated Ultrasensitive Electrochemical Immunoassay. *Anal. Chem.* **2016**, *88*, 12516−12523.
(36) Ling, P.; Lei, J.; Ju, H. Nanoscaled Porphyrinic Metal−Organic Frameworks for Electrochemical Detection of Telomerase Activity via Telomerase Triggered Conformation Switch. *Anal. Chem.* **2016**, *88*, 10680−10686.
(37) Zhan, W.-w.; Kuang, Q.; Zhou, J.-z.; Kong, Z.-j.; Xie, Z.-x.; Zheng, L.-s. Semiconductor@Metal−Organic Framework Core−Shell Heterostructures: A Case of ZnO@ZIF-8 Nanorods with Selective Photoelectrochemical Response. *J. Am. Chem. Soc.* **2013**, *135*, 1926−1933.
(38) Zhang, G.-Y.; Zhuang, Y.-H.; Shan, D.; Su, G.-F.; Cosnier, S.; Zhang, X.-J. Zirconium-Based Porphyrinic Metal−Organic Framework (PCN-222): Enhanced Photoelectrochemical Response and Its Application for Label-Free Phosphoprotein Detection. *Anal. Chem.* **2016**, *88*, 11207−11212.
(39) Yu, Y. M.; Zhang, J. H.; Xiao, C. H.; Zhong, J. D.; Zhang, X. H.; Chen, J. H. High Active Hollow Nitrogen-Doped Carbon Microspheres for Oxygen Reduction in Alkaline Media. *Fuel Cells* **2012**, *12*, 506−510.
(40) Gai, P.; Zhang, H.; Zhang, Y.; Liu, W.; Zhu, G.; Zhang, X.; Chen, J. Simultaneous Electrochemical Detection of Ascorbic Acid, Dopamine and Uric Acid Based on Nitrogen Doped Porous Carbon Nanopolyhedra. *J. Mater. Chem. B* **2013**, *1*, 2742−2749.
(41) Zeng, X.; Huang, L.; Wang, C.; Wang, J.; Li, J.; Luo, X. Sonocrystallization of ZIF-8 on Electrostatic Spinning TiO_2 Nanofibers Surface with Enhanced Photocatalysis Property through Synergistic Effect. *ACS Appl. Mater. Interfaces* **2016**, *8*, 20274−20282.
(42) Kuang, Y.; Shi, J.; Li, J.; Yuan, D.; Alberti, K. A.; Xu, Q.; Xu, B. Pericellular Hydrogel/Nanonets Inhibit Cancer Cells. *Angew. Chem., Int. Ed.* **2014**, *53*, 8104−8107.
(43) Pires, R. A.; Abul-Haija, Y. M.; Costa, D. S.; Novoa-Carballal, R.; Reis, R. L.; Ulijn, R. V.; Pashkuleva, I. Controlling Cancer Cell Fate Using Localized Biocatalytic Self-Assembly of an Aromatic Carbohydrate Amphiphile. *J. Am. Chem. Soc.* **2015**, *137*, 576−579.
(44) Li, G.; Fu, H.; Chen, X.; Gong, P.; Chen, G.; Xia, L.; Wang, H.; You, J.; Wu, Y. Facile and Sensitive Fluorescence Sensing of Alkaline Phosphatase Activity with Photoluminescent Carbon Dots Based on Inner Filter Effect. *Anal. Chem.* **2016**, *88*, 2720−2726.
(45) Liu, Y.; Xiong, E.; Li, X.; Li, J.; Zhang, X.; Chen, J. Sensitive Electrochemical Assay of Alkaline Phosphatase Activity Based on TdT-

DOI: 10.1021/acsami.7b10856
ACS Appl. Mater. Interfaces 2017, 9, 42482−42491

Mediated Hemin/G-quadruplex DNAzyme Nanowires for Signal Amplification. *Biosens. Bioelectron.* **2017**, *87*, 970−975.
(46) Ma, J.-L.; Yin, B.-C.; Wu, X.; Ye, B.-C. Copper-Mediated DNA-Scaffolded Silver Nanocluster on−off Switch for Detection of Pyrophosphate and Alkaline Phosphatase. *Anal. Chem.* **2016**, *88*, 9219−9225.
(47) Gu, X.; Zhang, G.; Wang, Z.; Liu, W.; Xiao, L.; Zhang, D. A New Fluorometric Turn-on Assay for Alkaline Phosphatase and Inhibitor Screening Based on Aggregation and Deaggregation of Tetraphenylethylene Molecules. *Analyst* **2013**, *138*, 2427−2431.
(48) Díaz, A. N.; Sánchez, F. G.; Ramos, M. C.; Torijas, M. C. Horseradish Peroxidase Sol−Gel Immobilized for Chemiluminescence Measurements of Alkaline-Phosphatase Activity. *Sens. Actuators, B* **2002**, *82*, 176−179.
(49) Jiang, H.; Wang, X. Alkaline Phosphatase-Responsive Anodic Electro-chemiluminescence of CdSe Nanoparticles. *Anal. Chem.* **2012**, *84*, 6986−6993.
(50) Nie, F.; Luo, K.; Zheng, X.; Zheng, J.; Song, Z. Novel Preparation and Electrochemiluminescence Application of Luminol Functional-Au Nanoclusters for ALP Determination. *Sens. Actuators, B* **2015**, *218*, 152−159.
(51) Gao, Z.; Deng, K.; Wang, X.-D.; Miró, M.; Tang, D. High-Resolution Colorimetric Assay for Rapid Visual Readout of Phosphatase Activity Based on Gold/Silver Core/Shell Nanorod. *ACS Appl. Mater. Interfaces* **2014**, *6*, 18243−18250.
(52) Li, C. M.; Zhen, S. J.; Wang, J.; Li, Y. F.; Huang, C. Z. A Gold Nanoparticles-Based Colorimetric Assay for Alkaline Phosphatase Detection with Tunable Dynamic Range. *Biosens. Bioelectron.* **2013**, *43*, 366−371.
(53) Jiang, Z.; Sun, H.; Qin, Z.; Jiao, X.; Chen, D. Synthesis of Novel ZnS Nanocages Utilizing ZIF-8 Polyhedral Template. *Chem. Commun.* **2012**, *48*, 3620−3622.
(54) Shi, X.-M.; Fan, G.-C.; Shen, Q.; Zhu, J.-J. Photoelectrochemical DNA Biosensor Based on Dual-Signal Amplification Strategy Integrating Inorganic−Organic Nanocomposites Sensitization with λ-Exonuclease-Assisted Target Recycling. *ACS Appl. Mater. Interfaces* **2016**, *8*, 35091−35098.
(55) Wang, H.; Gao, Q.; Hu, J. High Hydrogen Storage Capacity of Porous Carbons Prepared by Using Activated Carbon. *J. Am. Chem. Soc.* **2009**, *131*, 7016−7022.
(56) Li, Y.; Liu, J.; Chen, C.; Zhang, X.; Chen, J. Preparation of NiCoP Hollow Quasi-Polyhedra and Their Electrocatalytic Properties for Hydrogen Evolution in Alkaline Solution. *ACS Appl. Mater. Interfaces* **2017**, *9*, 5982−5991.
(57) Liu, B.; Shioyama, H.; Akita, T.; Xu, Q. Metal−Organic Framework as a Template for Porous Carbon Synthesis. *J. Am. Chem. Soc.* **2008**, *130*, 5390−5391.
(58) Chen, W.; Zhang, X.; Ai, F.; Yang, X.; Zhu, G.; Wang, F. Graphitic Carbon Nanocubes Derived from ZIF-8 for Photothermal Therapy. *Inorg. Chem.* **2016**, *55*, 5750−5752.
(59) Guo, X.; Li, L.; Zhang, X.; Chen, J. Platinum Nanoparticles Encapsulated in Nitrogen-Doped Mesoporous Carbons as Methanol-Tolerant Oxygen Reduction Electrocatalysts. *ChemElectroChem* **2015**, *2*, 404−411.
(60) Zhou, M.; Gao, X.; Hu, Y.; Chen, J.; Hu, X. Uniform Hamburger-Like Mesoporous Carbon-Incorporated ZnO Nanoarchitectures: One-Pot Solvothermal Synthesis, High Adsorption and Visible-Light Photocatalytic Decolorization of Dyes. *Appl. Catal., B* **2013**, *138−139*, 1−8.
(61) Bai, F.; Xia, Y.; Chen, B.; Su, H.; Zhu, Y. Preparation and Carbon Dioxide Uptake Capacity of N-doped Porous Carbon Materials Derived from Direct Carbonization of Zeolitic Imidazolate Framework. *Carbon* **2014**, *79*, 213−226.
(62) Liang, C.; Li, Z.; Dai, S. Mesoporous Carbon Materials: Synthesis and Modification. *Angew. Chem., Int. Ed.* **2008**, *47*, 3696−3717.
(63) Powar, S.; Daeneke, T.; Ma, M. T.; Fu, D.; Duffy, N. W.; Götz, G.; Weidelener, M.; Mishra, A.; Bäuerle, P.; Spiccia, L.; Bach, U. Highly Efficient P-Type Dye-Sensitized Solar Cells Based on Tris(1,2-diaminoethane)Cobalt(II)/(III) Electrolytes. *Angew. Chem., Int. Ed.* **2013**, *52*, 602−605.
(64) Cooper, D. R.; Dimitrijevic, N. M.; Nadeau, J. L. Photosensitization of CdSe/ZnS QDs and Reliability of Assays for Reactive Oxygen Species Production. *Nanoscale* **2010**, *2*, 114−121.
(65) Bao, L.; Sun, L.; Zhang, Z.-L.; Jiang, P.; Wise, F. W.; Abruña, H. D.; Pang, D.-W. Energy-Level-Related Response of Cathodic Electrogenerated-Chemiluminescence of Self-Assembled CdSe/ZnS Quantum Dot Films. *J. Phys. Chem. C* **2011**, *115*, 18822−18828.
(66) Cao, Y.; Zhu, S.; Yu, J.; Zhu, X.; Yin, Y.; Li, G. Protein Detection Based on Small Molecule-Linked DNA. *Anal. Chem.* **2012**, *84*, 4314−4320.
(67) Zhang, N.; Ma, Z.-Y.; Ruan, Y.-F.; Zhao, W.-W.; Xu, J.-J.; Chen, H.-Y. Simultaneous Photoelectrochemical Immunoassay of Dual Cardiac Markers Using Specific Enzyme Tags: A Proof of Principle for Multiplexed Bioanalysis. *Anal. Chem.* **2016**, *88*, 1990−1994.
(68) Deng, J.; Yu, P.; Wang, Y.; Mao, L. Real-Time Ratiometric Fluorescent Assay for Alkaline Phosphatase Activity with Stimulus Responsive Infinite Coordination Polymer Nanoparticles. *Anal. Chem.* **2015**, *87*, 3080−3086.
(69) Jiao, H.; Chen, J.; Li, W.; Wang, F.; Zhou, H.; Li, Y.; Yu, C. Nucleic Acid-Regulated Perylene Probe-Induced Gold Nanoparticle Aggregation: A New Strategy for Colorimetric Sensing of Alkaline Phosphatase Activity and Inhibitor Screening. *ACS Appl. Mater. Interfaces* **2014**, *6*, 1979−1985.
(70) Zheng, F.; Guo, S.; Zeng, F.; Li, J.; Wu, S. Ratiometric Fluorescent Probe for Alkaline Phosphatase Based on Betaine-Modified Polyethylenimine via Excimer/Monomer Conversion. *Anal. Chem.* **2014**, *86*, 9873−9879.

DOI: 10.1021/acsami.7b10856
ACS Appl. Mater. Interfaces 2017, 9, 42482−42491